Main Features of the North American Monsoon

Francina Dominguez
Tereza Cavazos
Christopher Castro
Salvatore Pascale
Huancui Hu

August 19, 2019

Advanced School and Workshop on American Monsoons: progress and future plans

ICTP-SAIFR
São Paulo, SP Brazil

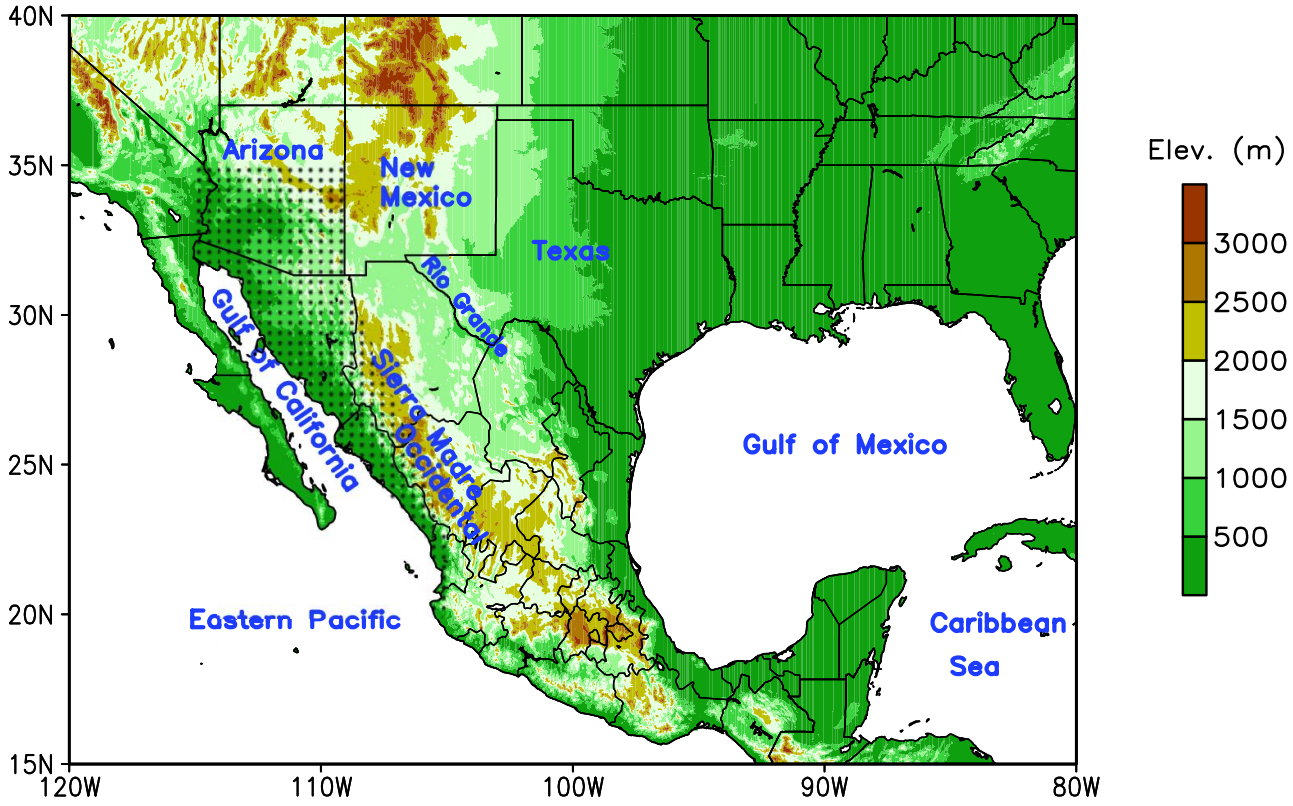

Climatology

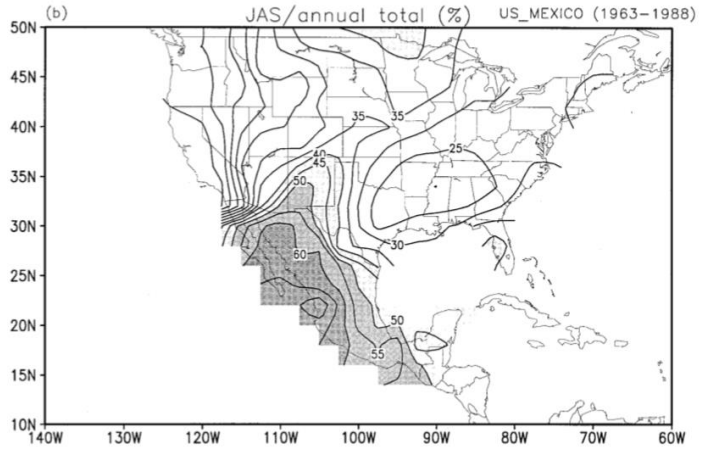

Variability

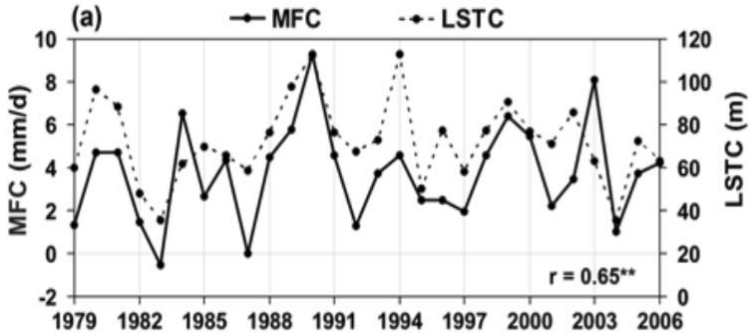

Changes

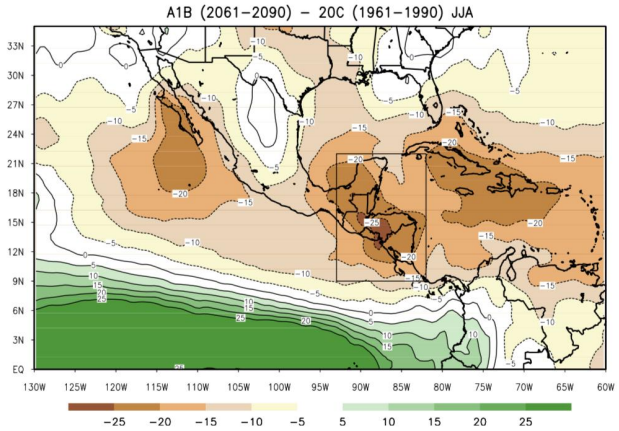

Climatology

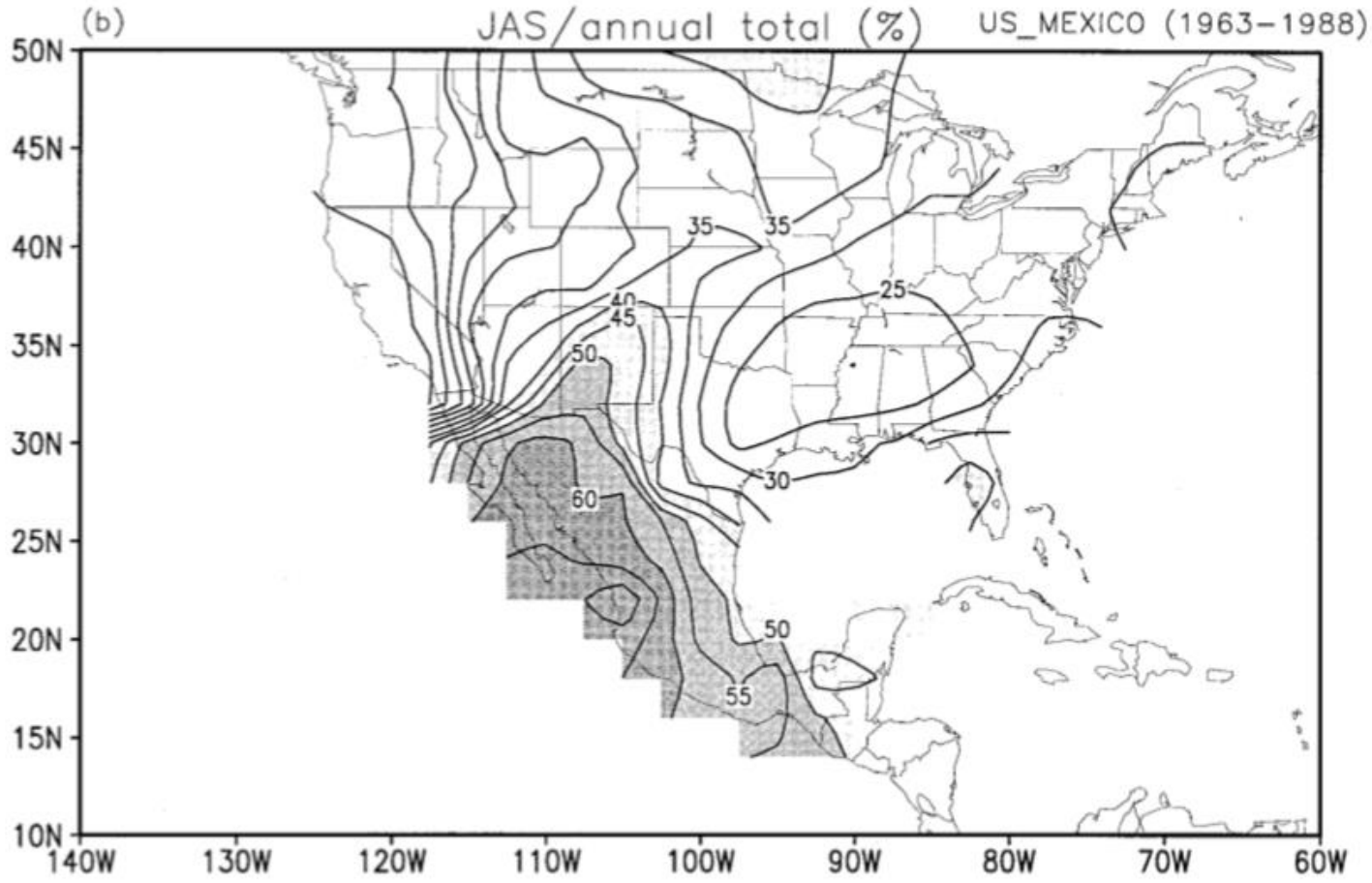

NAM precipitation accounts for more than 60% of total precipitation in the core monsoon region.

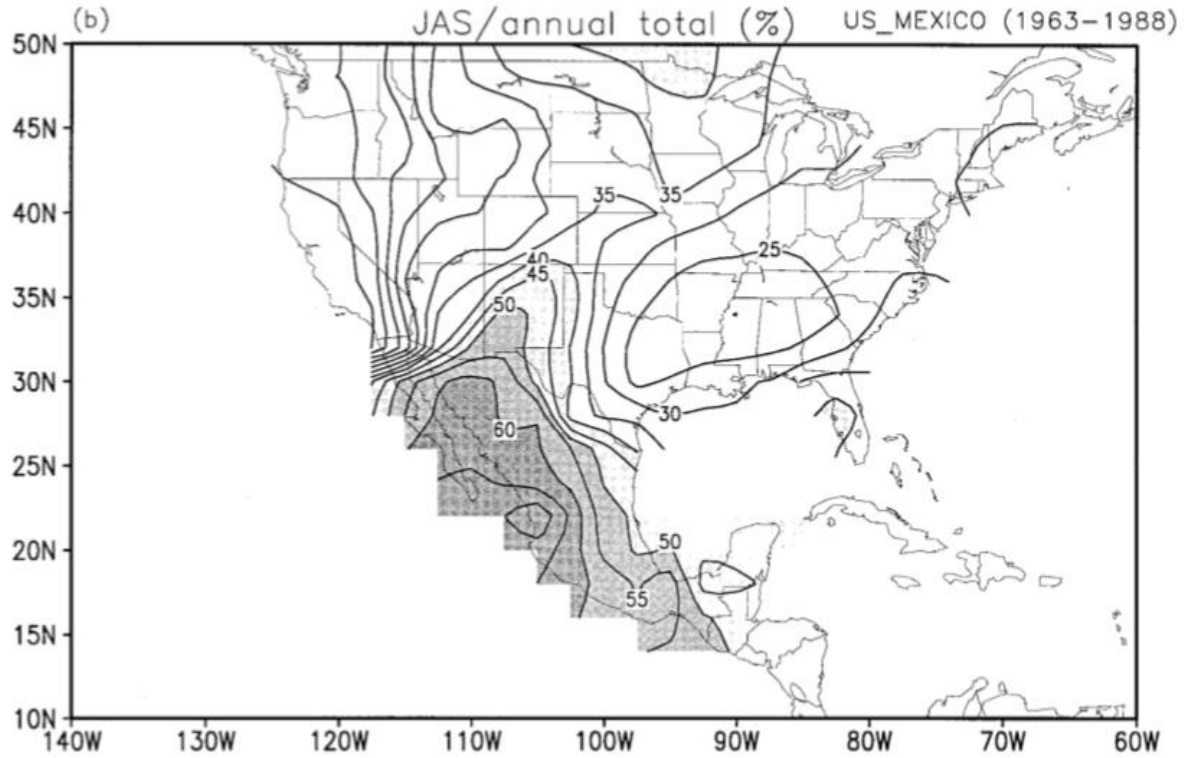

FIG. 5. (a) Mean (1963–88) seasonal precipitation (units: mm) for July–September from the US–MEXICO merged analysis. The contours are 50, 100, 200, 400, 600, 800, and 1000 mm and values greater than 100 mm are shaded. (b) Contribution of the precipitation during July–September to the annual total, expressed in percent, from the US–MEXICO merged precipitation analysis. The contour interval is 5% and values greater than 40% are shaded.

Higgins et al. 1999

NAM starts in June along the southwestern slopes on the Sierra Madre Occidental, moves north through Mexico by late June and reaches the southwestern USA in early July. Decays from mid-to-late September.

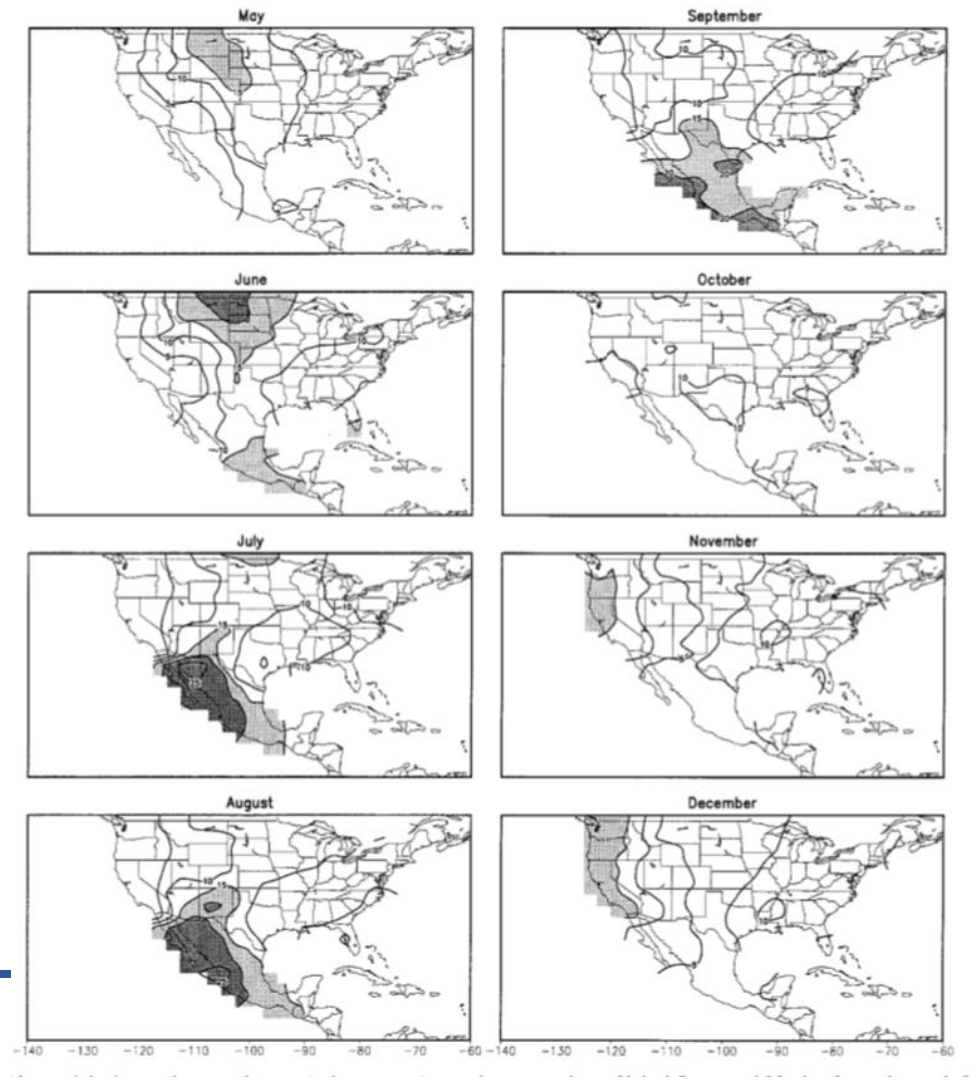

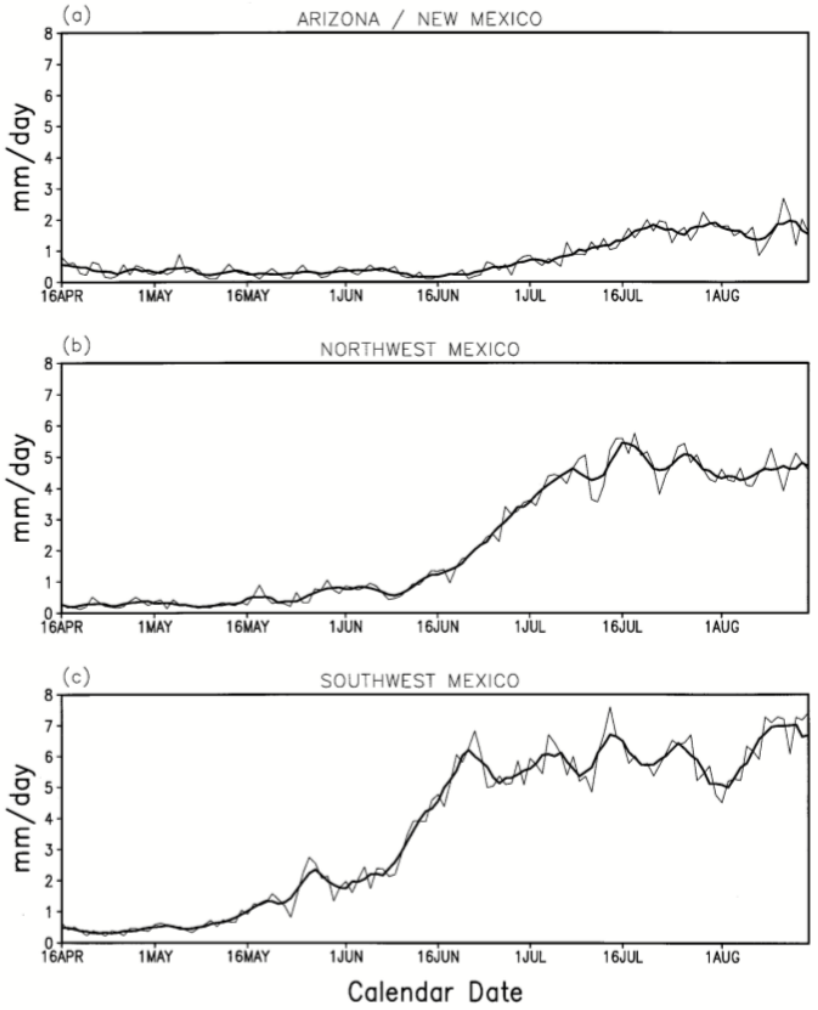

FIG. 3. Mean (1963–88) daily and 5-day running mean area averaged precipitation (units: mm day^{-1}) for the (a) AZNM, (b) NWMEX, and (c) SWMEX regions.

Higgins et al. 1999

The “monsoon high” related to enhanced atmospheric heating over the elevated terrain is characteristic of the NAM (analogous to the Bolivian High).

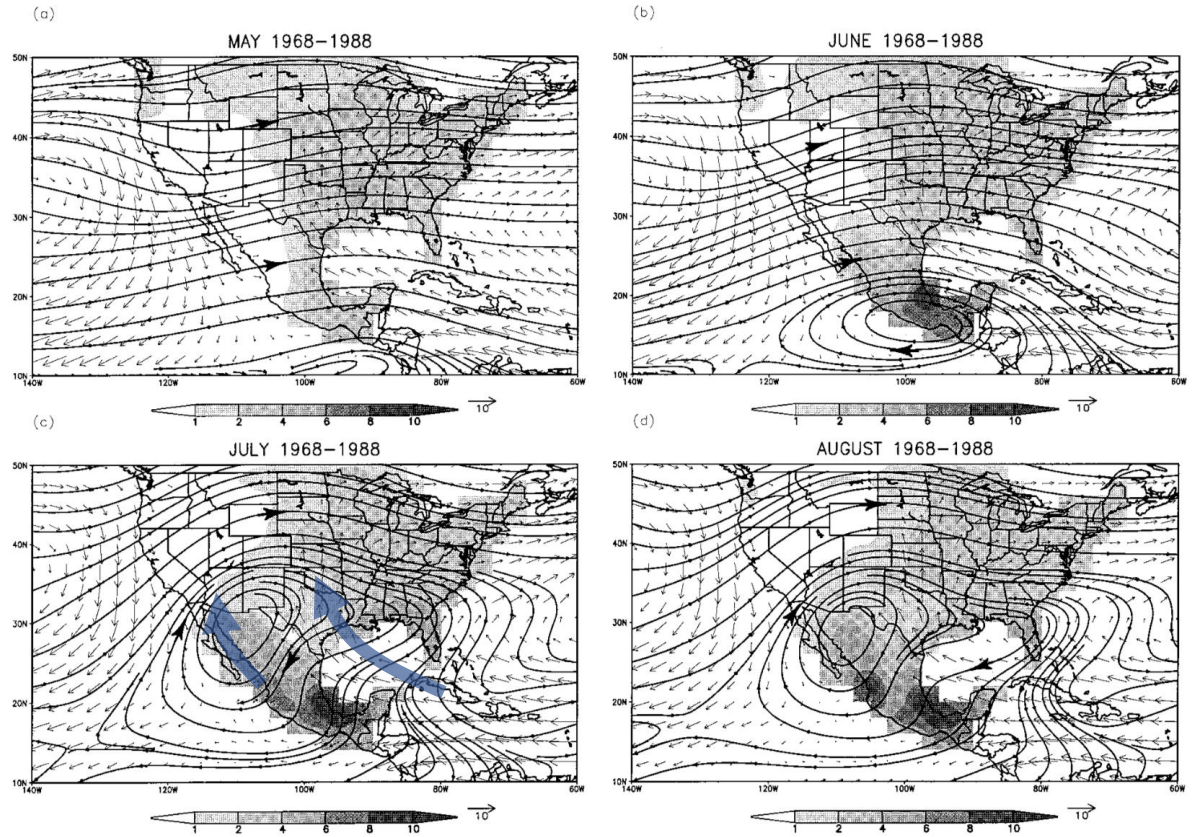

FIG. 7. Mean (1968–88) monthly 925-hPa vector wind (m s^{-1}), 200-hPa streamlines, and US–MEXICO precipitation (shading) for (a) May, (b) June, (c) July, and (d) August. Circulation data are from the NCEP–NCAR Reanalysis. A topography mask has been applied to the 925-hPa winds. Precipitation amounts are in mm day^{-1} and values greater than 1 mm day^{-1} are shaded. The characteristic vector length is 10 m s^{-1}.

Lower-level winds show the Gulf of California and Gulf of Mexico low-level jets.

Higgins et al. 1999

Until the late 1990's, oceans were thought to be the dominant source of NAM precipitation (Schmitz and Mullen, 1996).

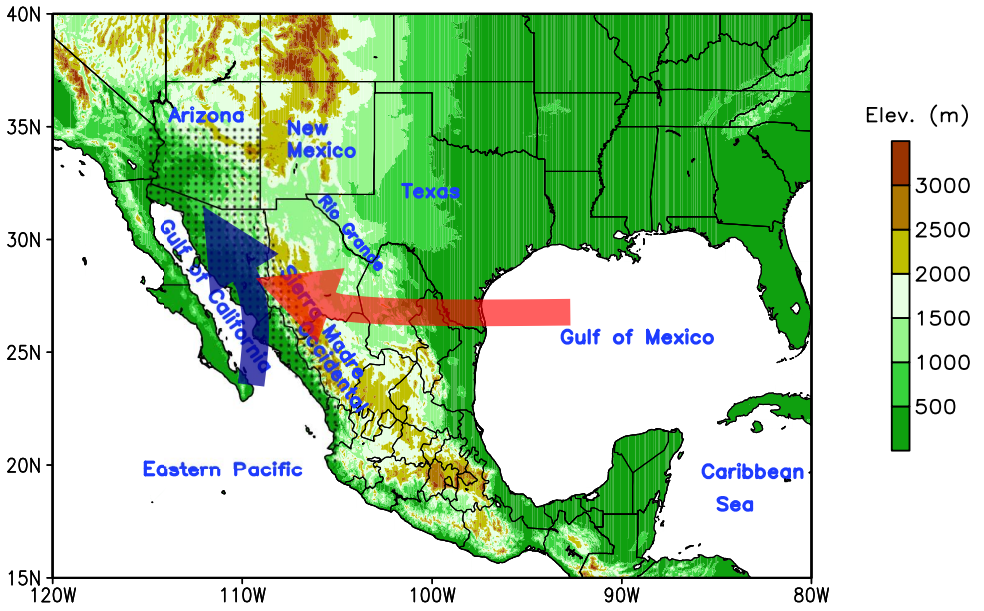

Then, GCMs with moisture tagging suggested a significant terrestrial contribution to NAM precipitation (Bosilovich et al. 2003)

Using the Dynamic Recycling Model over the North American Monsoon region.

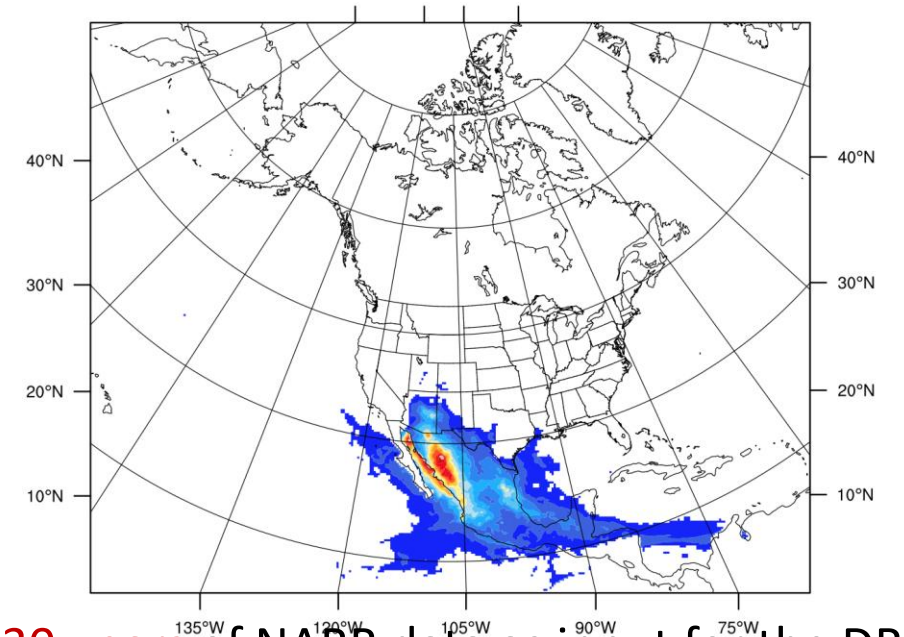

30-years of NARR data as input for the DRM

We can evaluate how much each “grid cell” contributes to NAM precipitation every day.

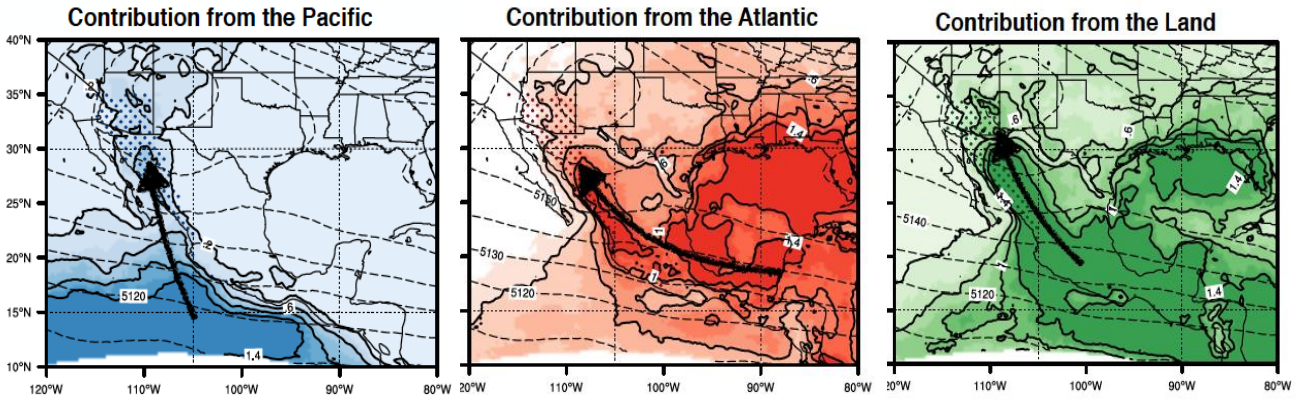

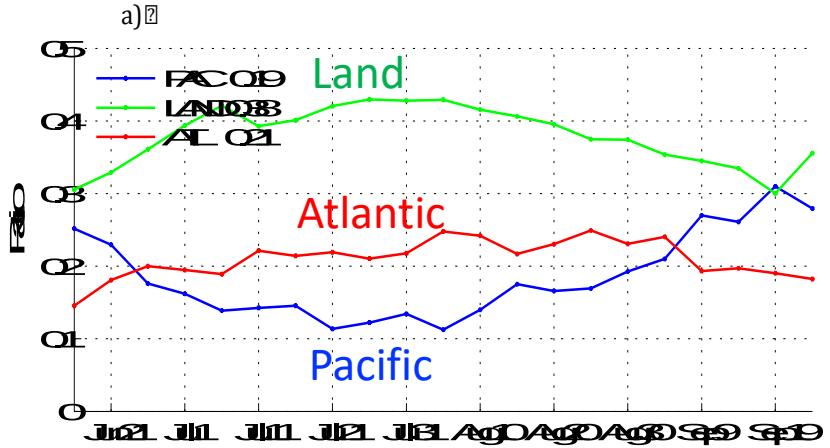

Terrestrial sources account for ~ 38% of precip. during the peak NAM season.

Hu and Dominguez, 2015

We also found a south-north progression of moisture sources.

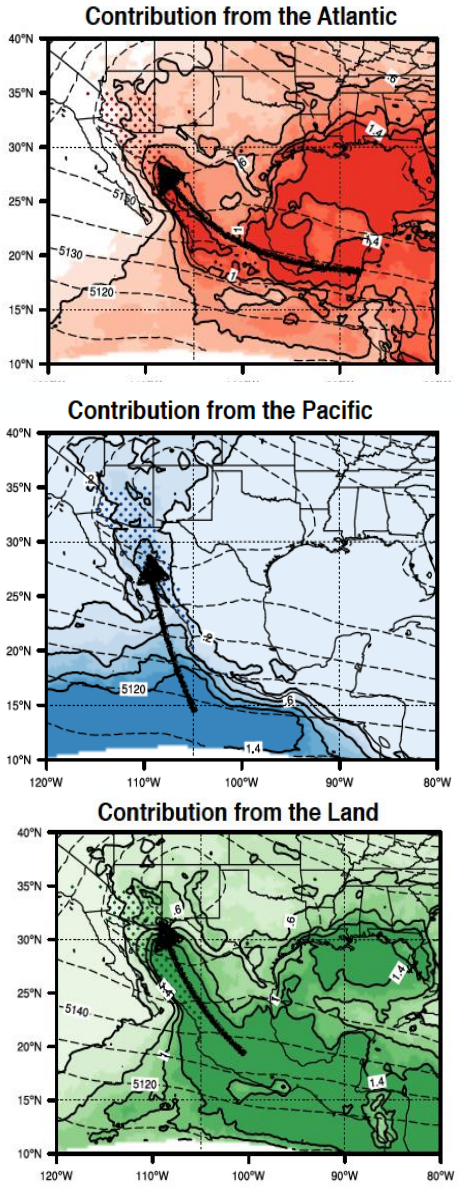

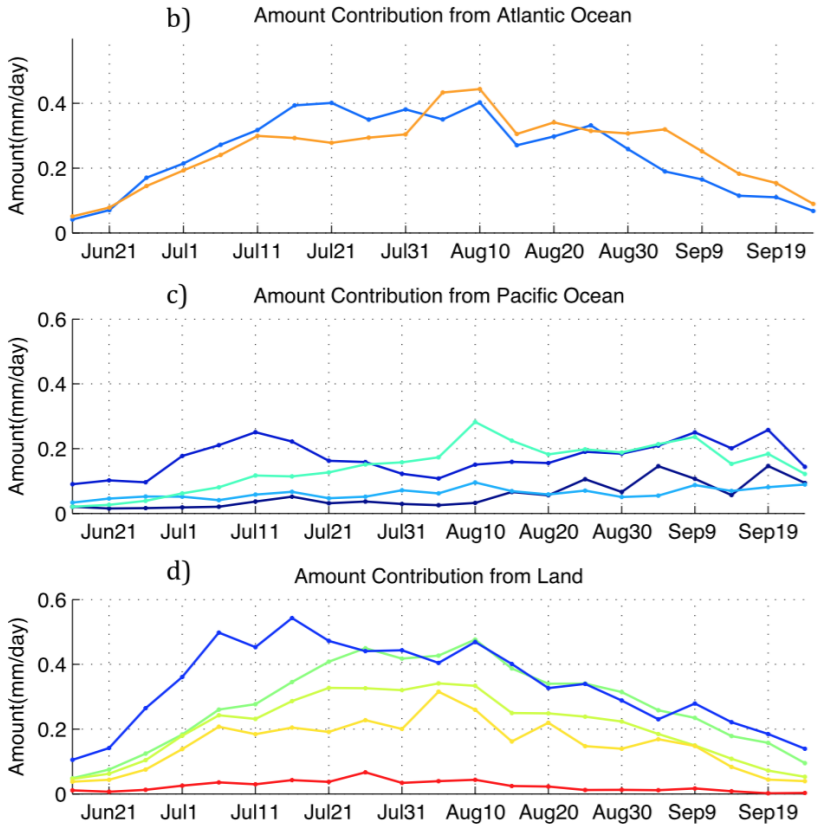

Caribbean Sea contributed to ~10%.

Tropical Pacific contributed to ~9%

Local recycling accounted for about ~10% while sources from Central America accounted for ~14%!

Hu and Dominguez, 2015

Variability

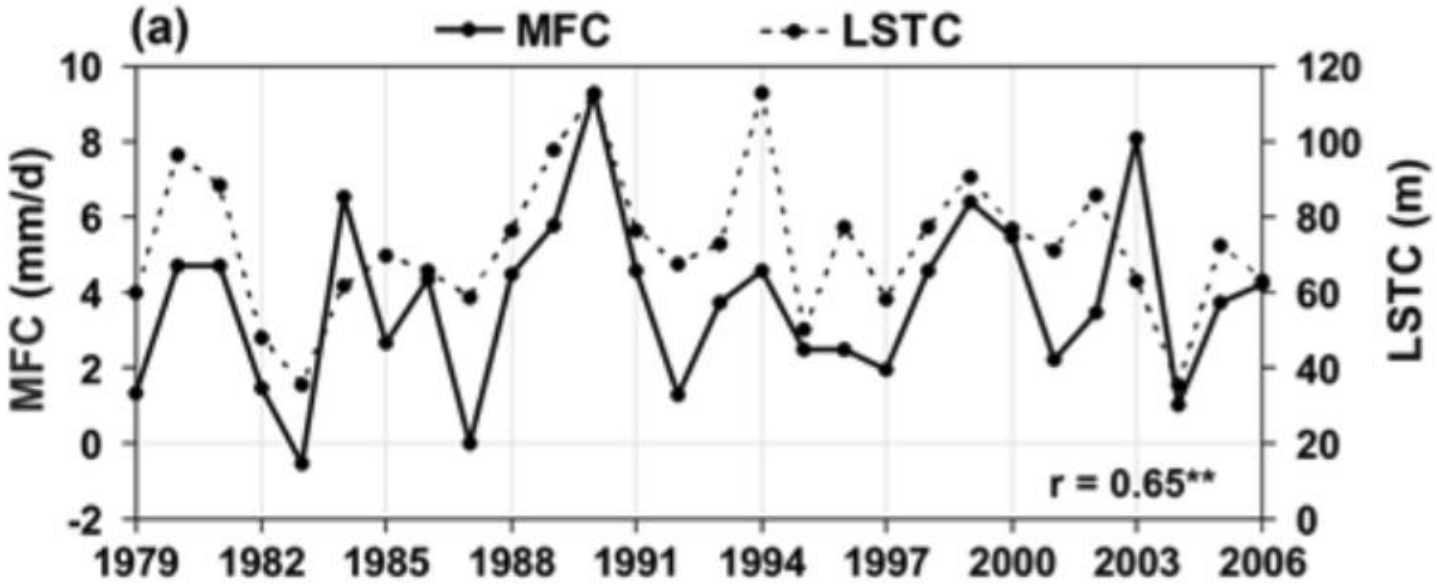

Thunderstorms initiate by air rising over mountain ranges in a conditionally unstable environment. The transition from shallow to deep convection occurs in mid-afternoon.

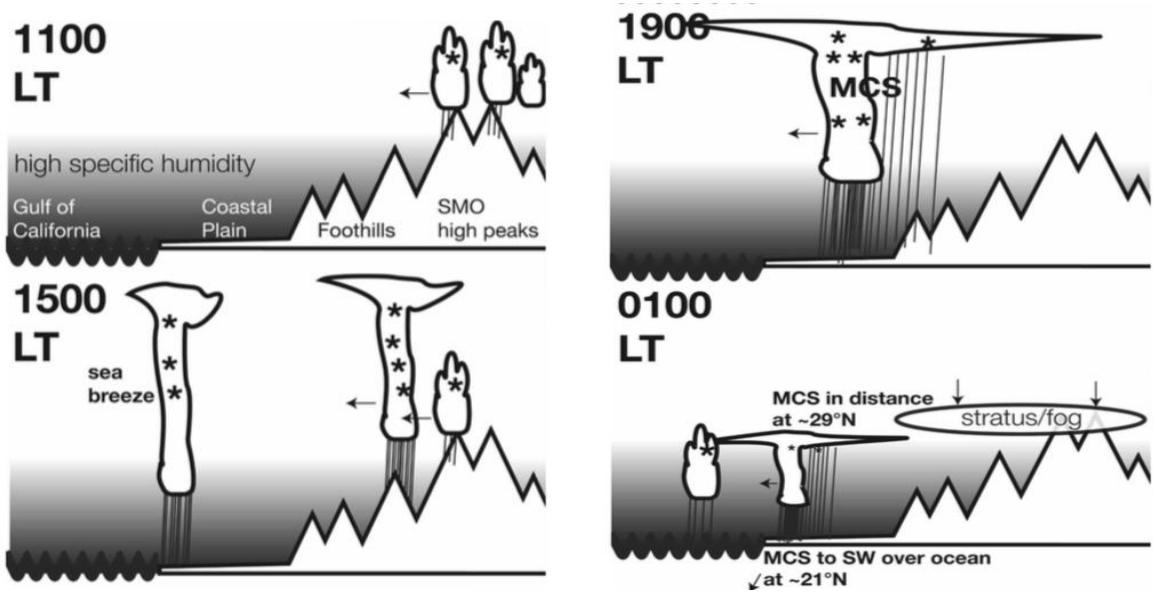

Schematic of observed diurnal mechanisms along the Sierra Madre Occidental at 25°N. Cloud type indicates relative height attained by clouds, shading indicates specific humidity contrasts, asterisks indicate mixed-phase microphysical processes, and the density of the vertical streaks indicates the locations and relative intensities of precipitation.

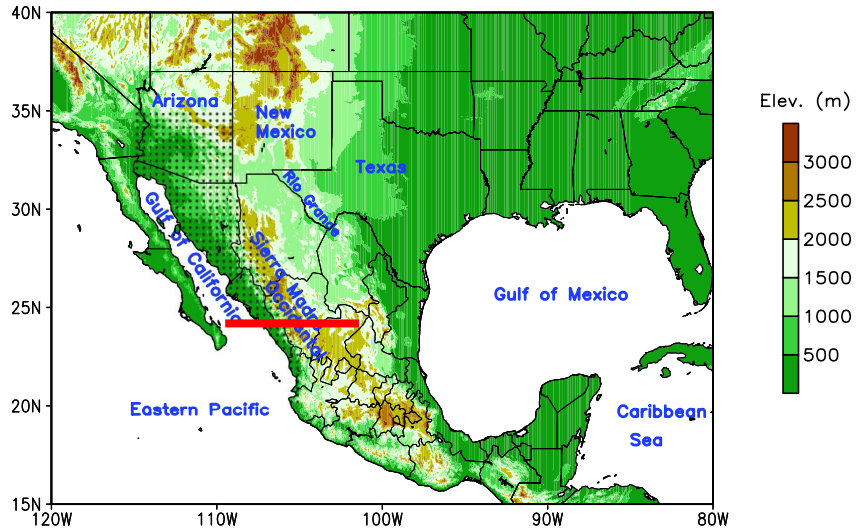

Nesbitt et al. 2008

There is a strong signature of occurrence of afternoon convection conditioned on morning time evaporative fraction, EF, the ratio of latent heating to the sum of latent and sensible fluxes.

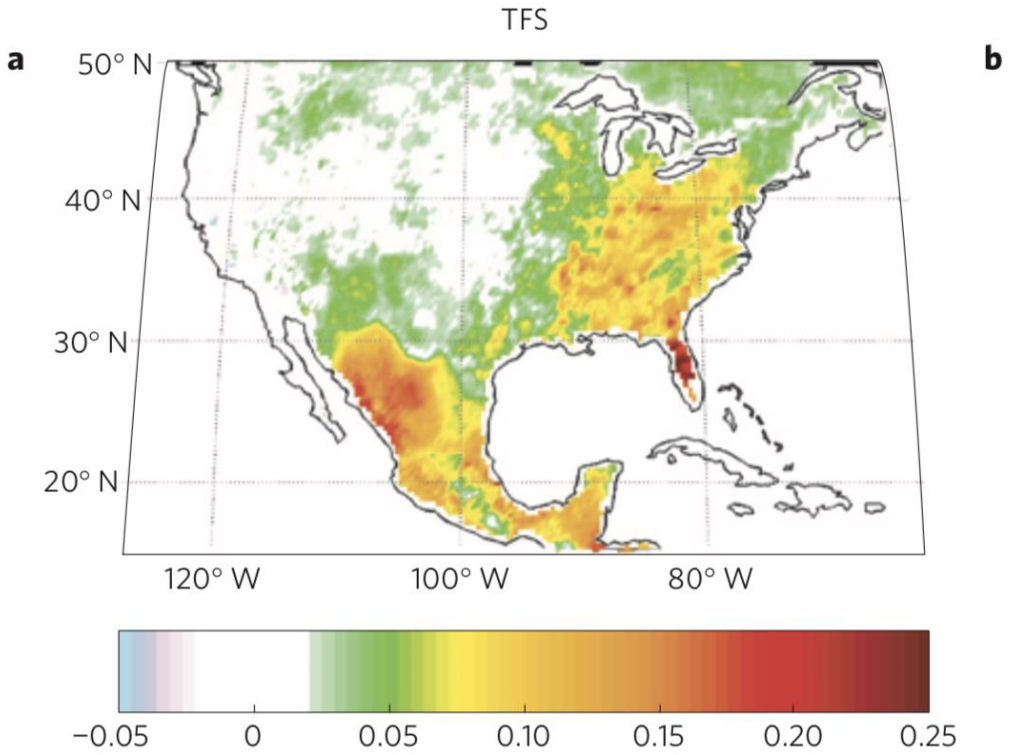

Findell et al. 2011

In fact, large percentage of moisture (13%) originates from the NAM region and precipitates back (recycled precipitation).

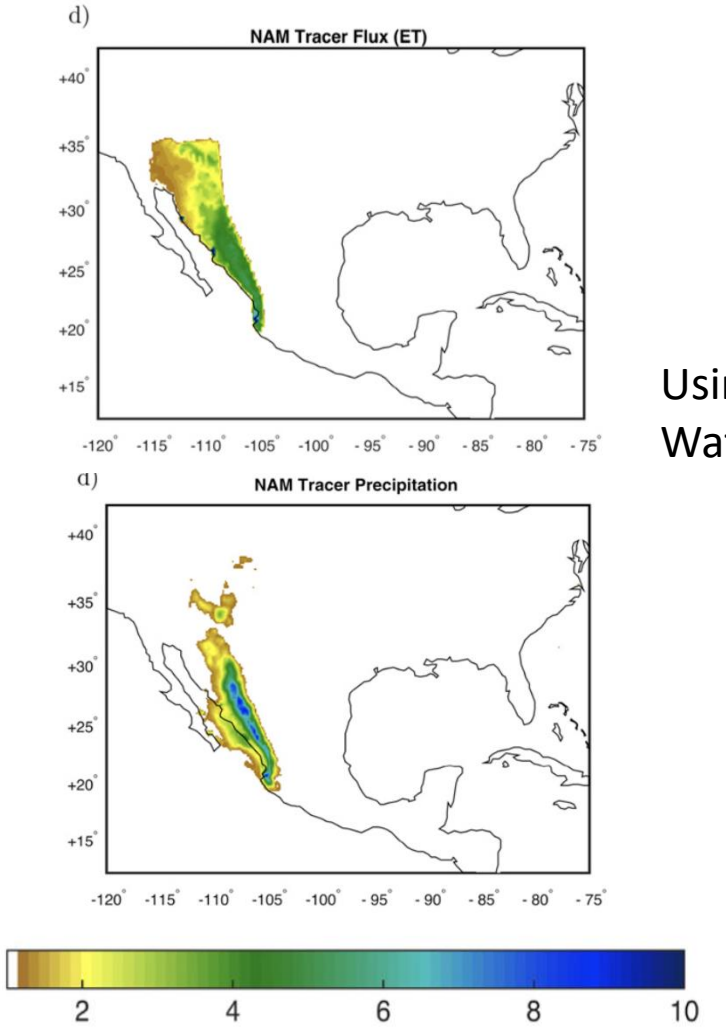

The moisture is very efficiently converted into precipitation.

Using WRF with
Water Vapor Tracers.

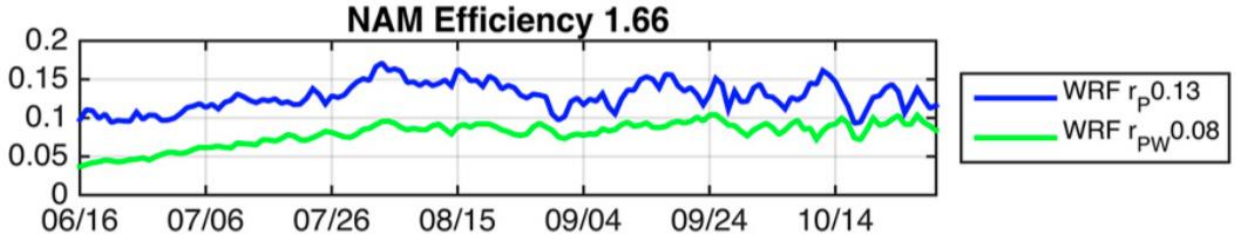

Evaporation (mm/day) and Precipitation (mm/day) originating from NAM evaporation

Dominguez et al. 2016

“Monsoon bursts”, intense thunderstorm activity, are associated with synoptic-scale phenomena: upper-level inverted troughs (IVs), gulf surges, tropical easterly waves (TEW) and tropical cyclones (TCs).

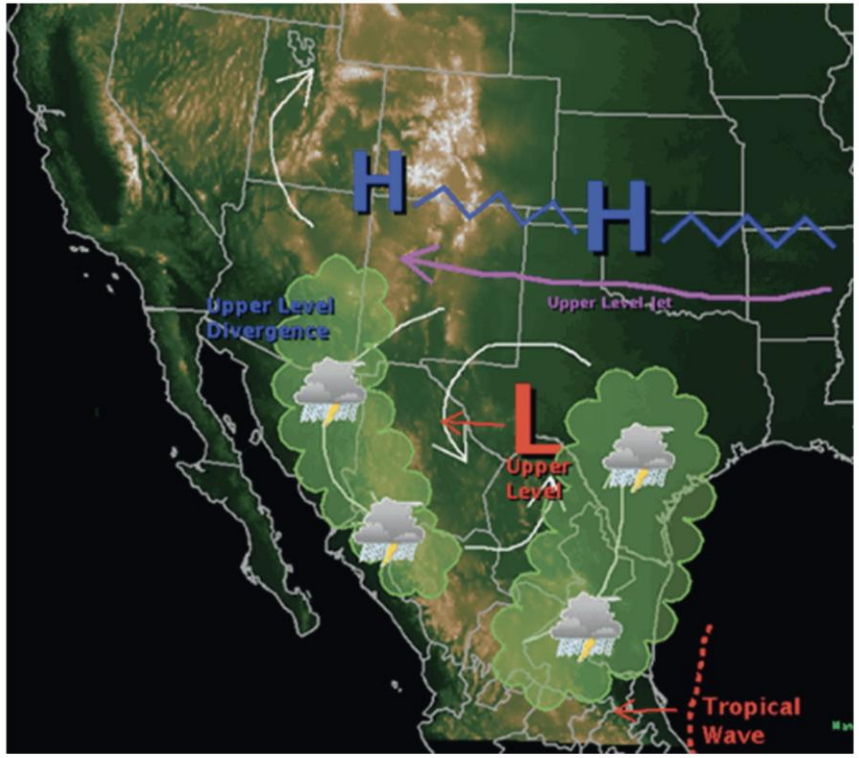

FIG. 3. Conceptual hypothesis of a subtropical upper-tropospheric low moving west into the North American monsoon regime, as adapted from Pytlak et al. (2005). The upper-level jet depicted in this figure is simply an enhanced easterly flow rather than a core of fast moving easterlies.

IVs are easterly moving upper-tropospheric cyclonic disturbances that are associated with quasi- geostrophic vertical motion and vorticity advection.

When an IV is in the region, storms move off the mountains into the lower terrain rather than dissipating thus facilitating severe weather.

Pytlak et al. 2005 and Bieda et al. 2009

Northward surges of moist air from the tropical Pacific via the Gulf of California are related to the amount of convective activity in north- western Mexico and portions of the southwestern United States.

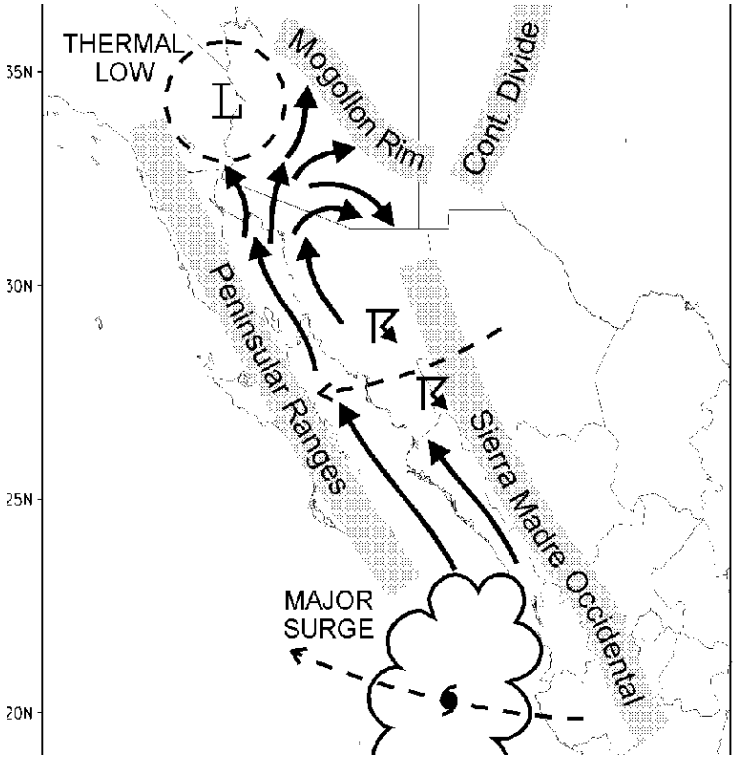

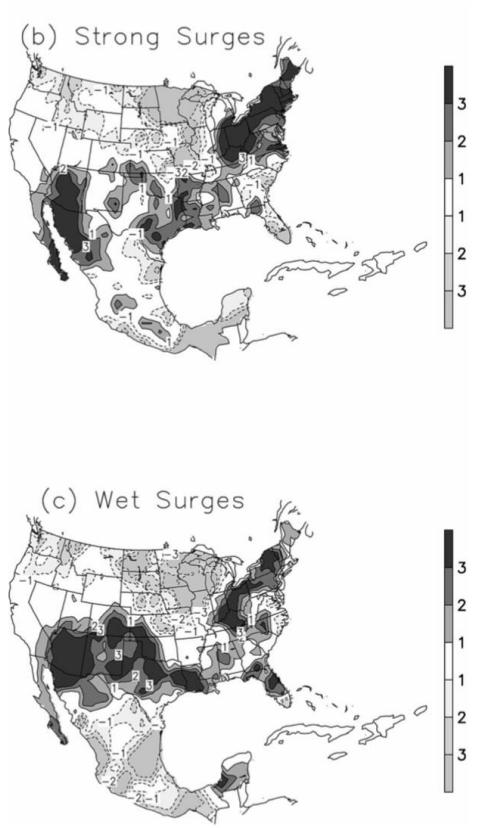

FIG. 8. Observed precipitation represented as the composite mean difference between the 5-day period after onset (day 0 to +4) and the 5-day period before onset (day −5 to −1) for (a) all, (b) strong, and (c) wet surges keyed to Yuma. The contour interval is 1 mm day^{-1}, the zero contour is omitted for clarity, and values greater than 1 mm day^{-1} (less than −1 mm day^{-1}) are shaded dark (light).

Higgins et al 2004

Tropical cyclones also carry a large quantity of tropical moisture and, upon interaction with mountainous topography, contribute to 30% of the local annual precipitation.

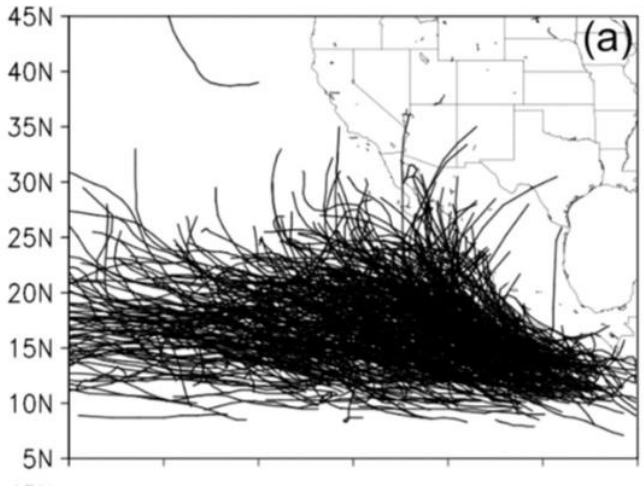

Wood and Ritchie 2013

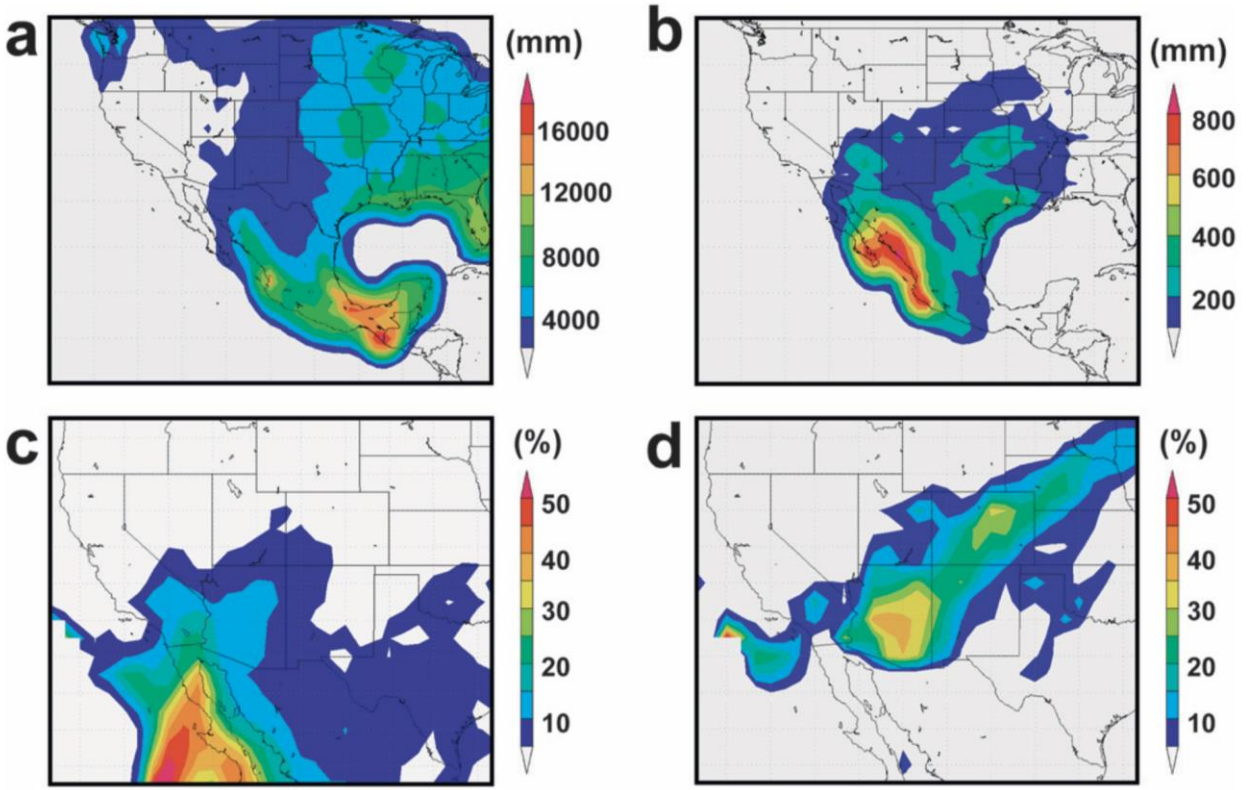

FIG. 3. Areal rainfall over the southwestern U.S. region calculated from the U.S.–Mexico unified gridded precipitation dataset: (a) total warm-season precipitation (15 Jun–31 Oct 1992–2005, mm), (b) total TC precipitation (1992–2005, mm), (c) percentage of warm-season precipitation due to TCs (1992–2005), and (d) percentage of warm-season precipitation due to TCs in 1992.

Ritchie et al. 2011

Zonal wind anomalies in the eastern tropical Pacific associated with the MJO tend to precede above-normal precipitation in the monsoon region of North America from several days to over a week later.

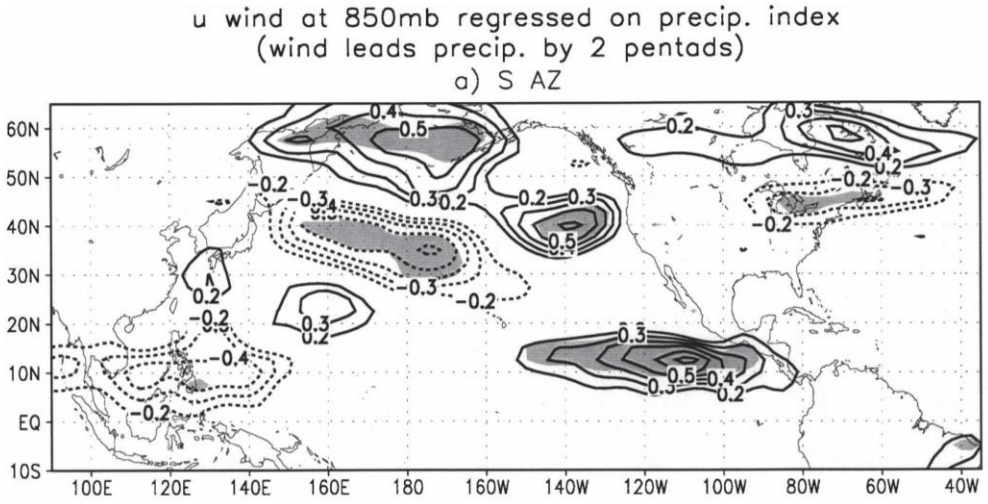

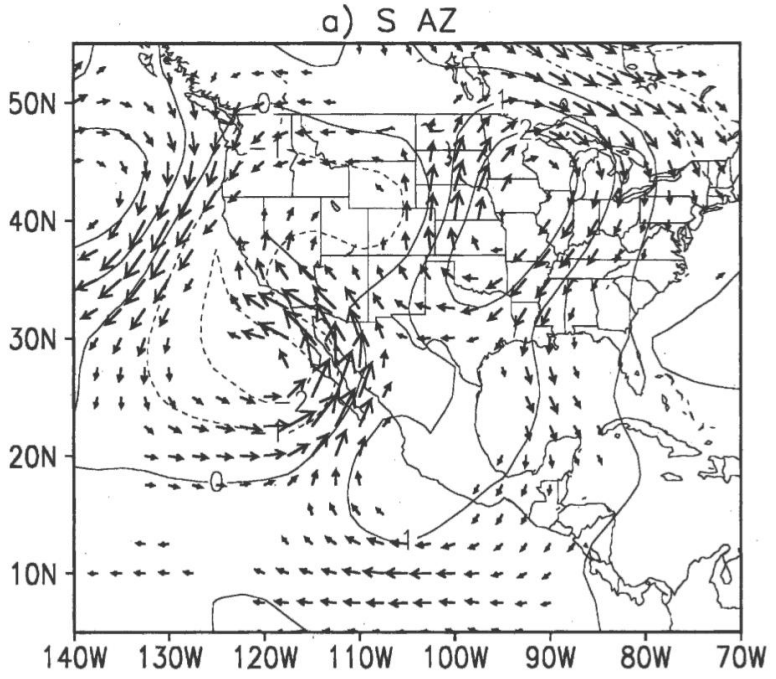

The MJO appears to contribute to the development of surges of moisture up the Gulf of California.

Lorenz and Hartmann 2006

Tropical and North Pacific SSTs are related to the occurrence of the teleconnection patterns in June and July.

A high (low) North Pacific Oscillation phase and El Niño (La Niña) conditions favor a weaker (stronger) and southward (northward) displaced monsoon ridge.

These teleconnection patterns affect the timing and large-scale distribution of monsoon moisture.

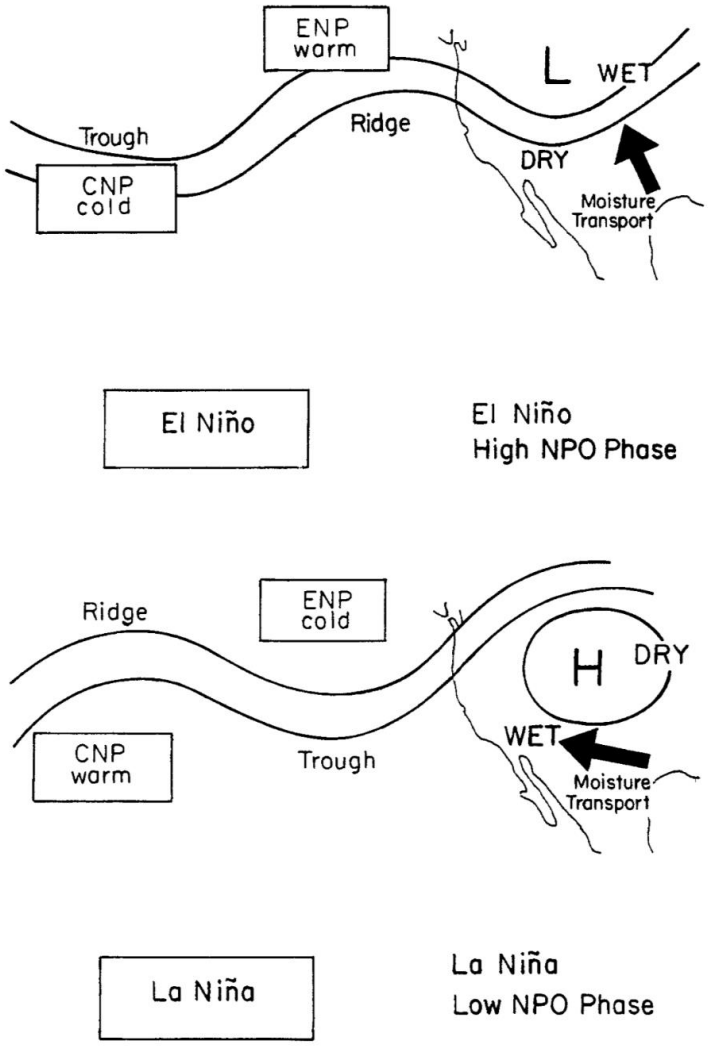

FIG. 14. Idealized relationship of monsoon ridge position and midlevel moisture transport to Pacific SSTs at monsoon onset.

Castro et al. 2001

Monsoon onset and interannual variability is found to be proportional land-sea temperature contrasts.

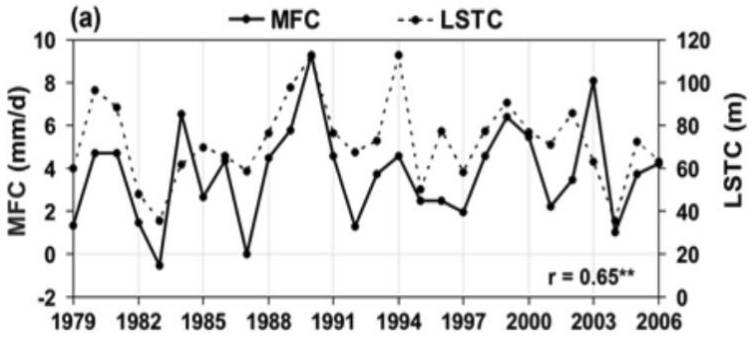

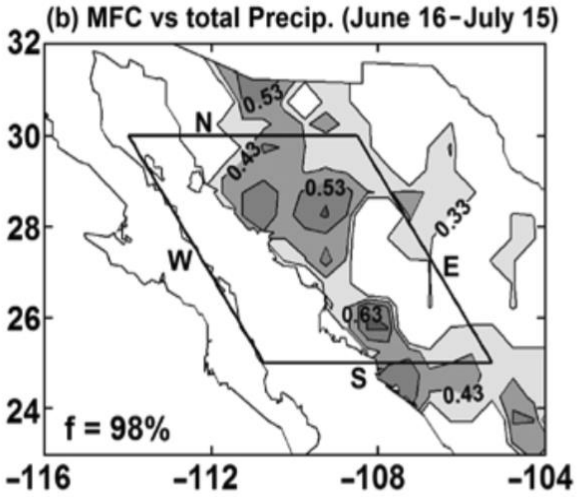

a) Time series of moisture flux convergence (MFC) and land-sea thermal contrast (LSTC) indices; the correlation coefficient (r) is statistically significant at the 99% level. b) Correlation between the MFC index and accumulated precipitation (June 16 - July 15) during the period 1979-2004; contour interval is 0.1; only significant contours ($p<0.05$) are plotted; f is the level of field significance.

The surface pressure gradient along the Gulf of California, and the ensuing low level moisture transport (from the southern Gulf of California and eastern tropical Pacific) and precipitation in the core region.

Turrent and Cavazos (2009)

Changes

Observed Changes

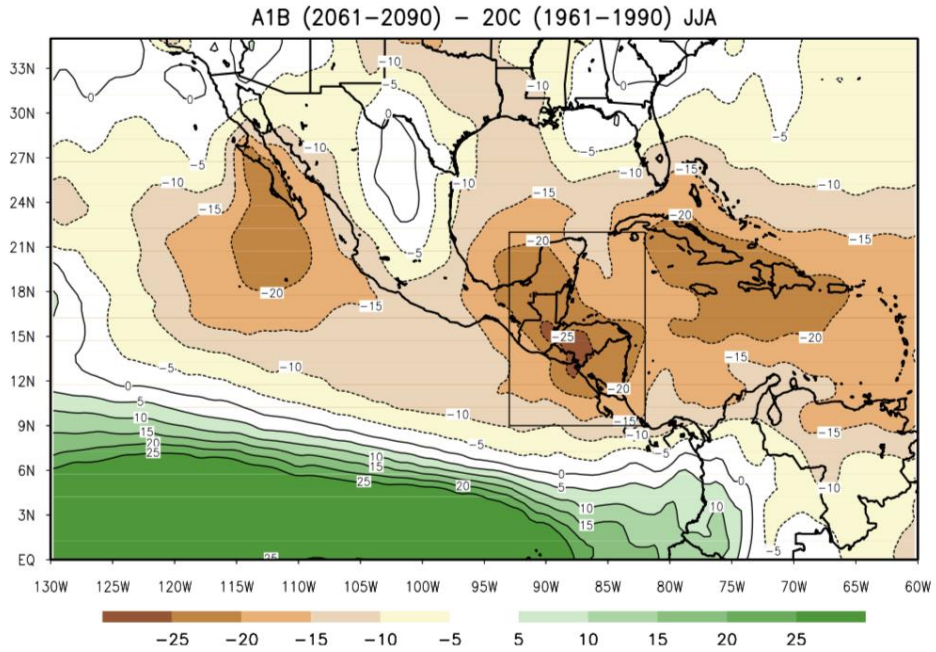

There has been a significant warming trend in the NAM region especially during winter and the summer months. The tails of the temperature distributions also show a significant increase.

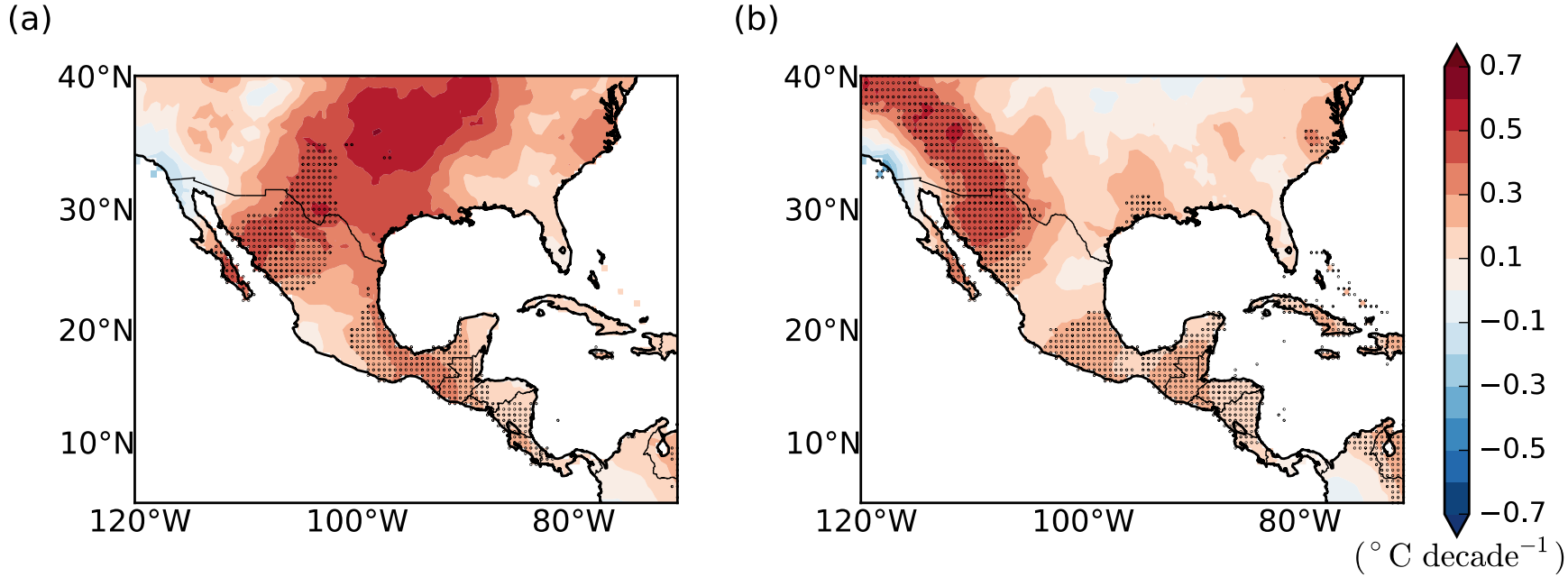

Figure 8. Observed CRU seasonal temperature trends (°C decade^{-1}) for (a) DJF and (b) JJA of 1980-2010. Statistical significant trends at the 95% level or greater are shown with dots.

Cavazos et al., 2019

Recent work with a very dense observational network of 59 rain gauges finds an increase in summer rainfall intensities in the region of southeastern Arizona beginning in the 1970s across a wide range of sub-daily time-scales.

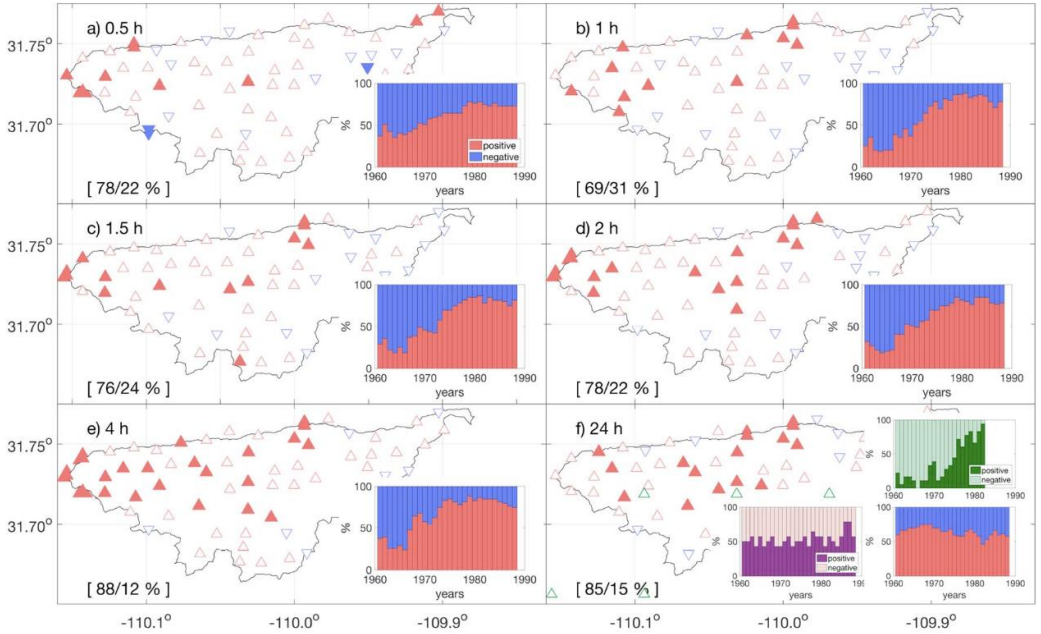

Figure 3. Spatial distribution of trends for the study period (map). The percentage of rain gauges with positive/negative trends is shown between brackets. The insets show percentage of rain gauges with positive/negative 30-year running trends. The Livneh/GHCN data sets are shown in green/purple in panel (f), respectively. Filled symbols denote statistically significant trends (10% level).

Demaria et al. 2019

There have been changes in the spatial distribution of IVs during the 1951–2010 analysis period, which are associated with a strengthening of the monsoon ridge.

It is suggested that IVs have played a lesser role in the initiation and organization of monsoon convection in the southwest CONUS during recent warm seasons.

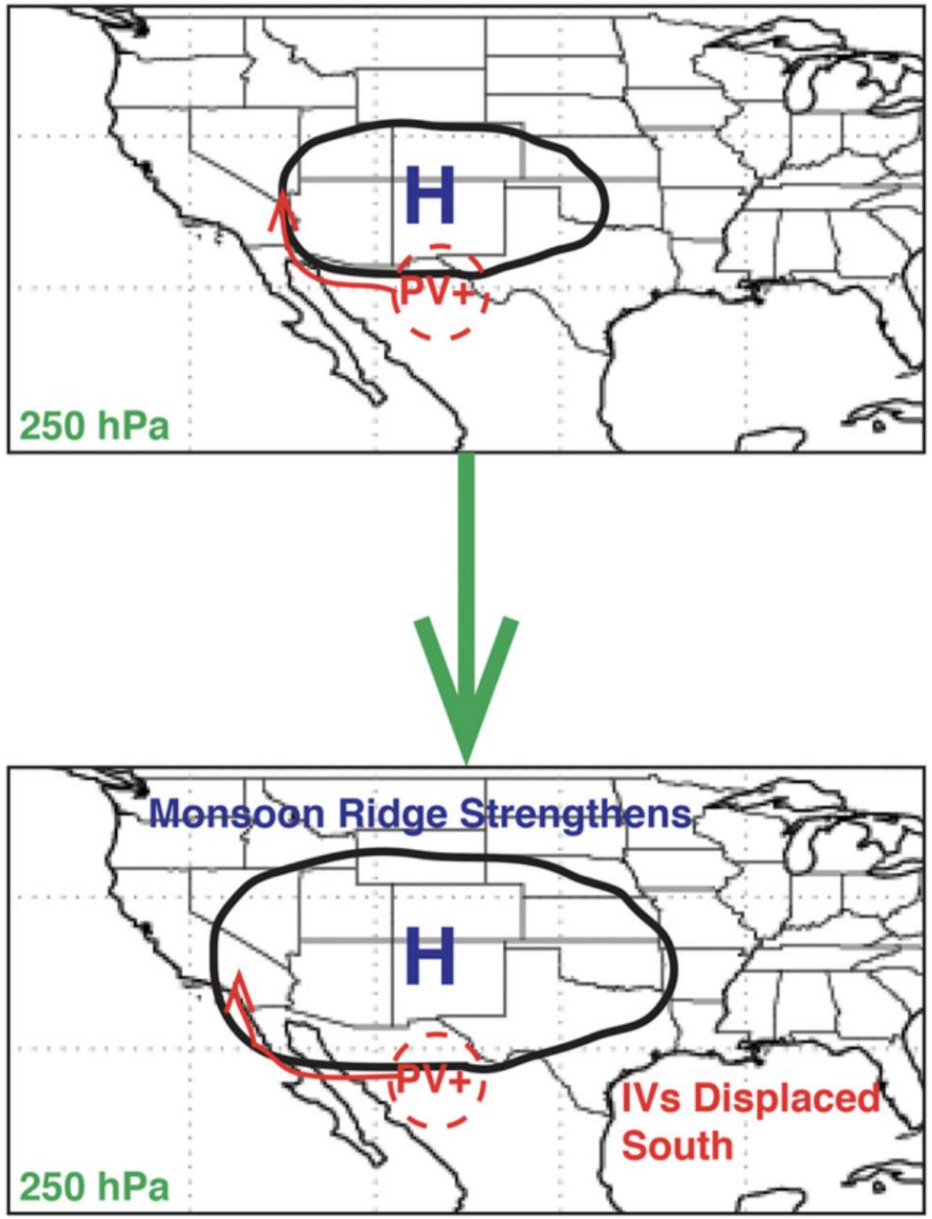

FIG. 18. Conceptual illustration of changing upper troposphere (250 hPa) dynamics during the NAM season. The strengthening monsoon high is displacing PV anomalies (IVs) away from its center.

Lahmers et al. 2016

Long-term increase in atmospheric moisture and instability is associated with an increase in extreme monsoon precipitation in observations and simulations of severe weather events. Precipitation is becoming more intense within the context of the diurnal cycle of convection.

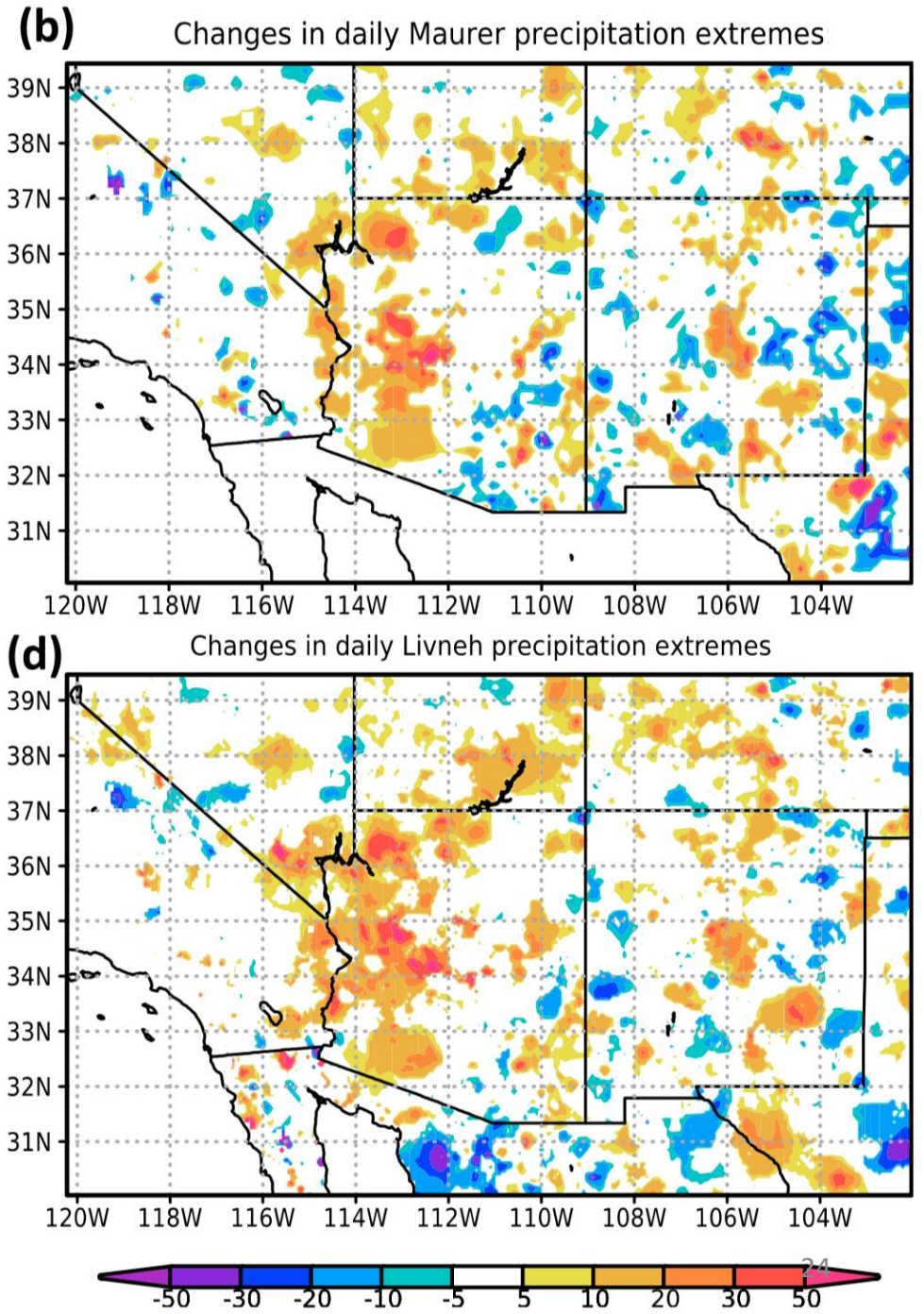

Luong et al. 2017

“NAM rainfall is becoming more 'thermodynamically dominated.’ It is more phase locked to the terrain and there is less tendency to organize and propagate. But when the fewer IV events do help to organize the convection, now those events tend to be more intense, because they are occurring in a more favorable thermodynamic environment.” Chris Castro, personal communication.

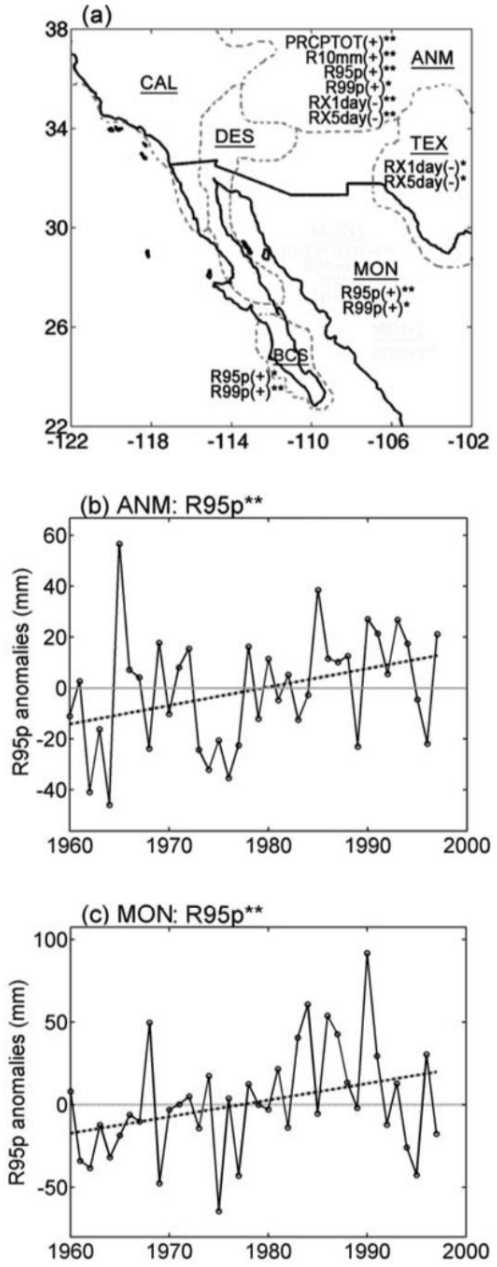

Figure 5. (a) Statistically significant annual trends in each of the six precipitation regions. Annual time series anomalies and linear trends (dashed lines) of R95p in (b) ANM and (c) MON. One (two) asterisks in Figure 5a indicate statistical significance at the 90% (95%) level.

The analysis of summer (June–October) daily precipitation indices also reveals the occurrence of significant positive trends in extreme precipitation in northwest Mexico mainly due to tropical cyclone activity.

Arriaga-Ramirez and Cavazos 2010

Changes

Projected Changes

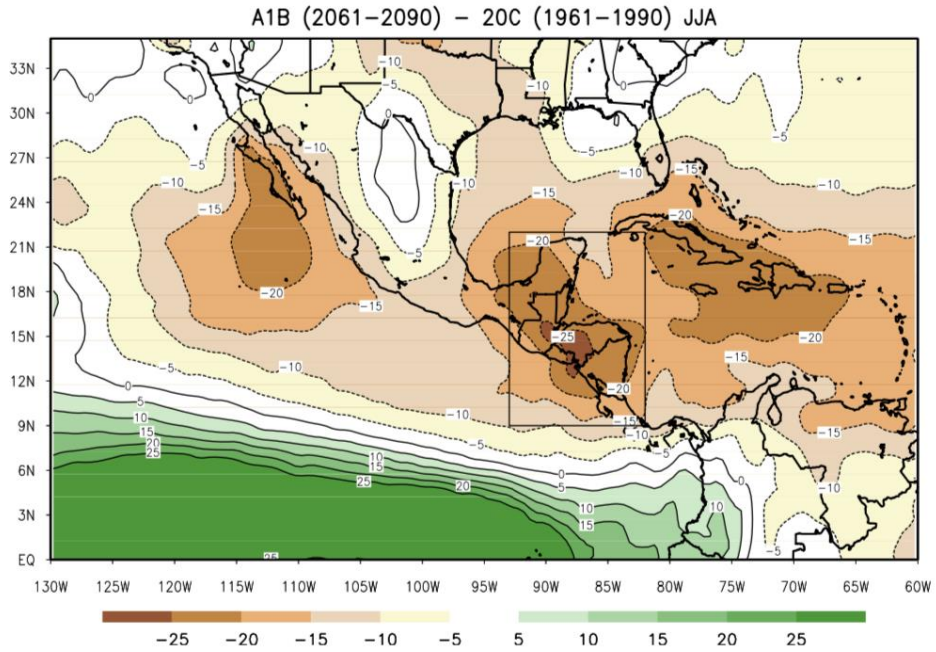

Analysis of CMIP5 GCMs show significant declines in early monsoon season precipitation (June-July) and increases in late monsoon season (September-October) precipitation, indicating a shift in seasonality toward delayed onset and withdrawal of the monsoon.

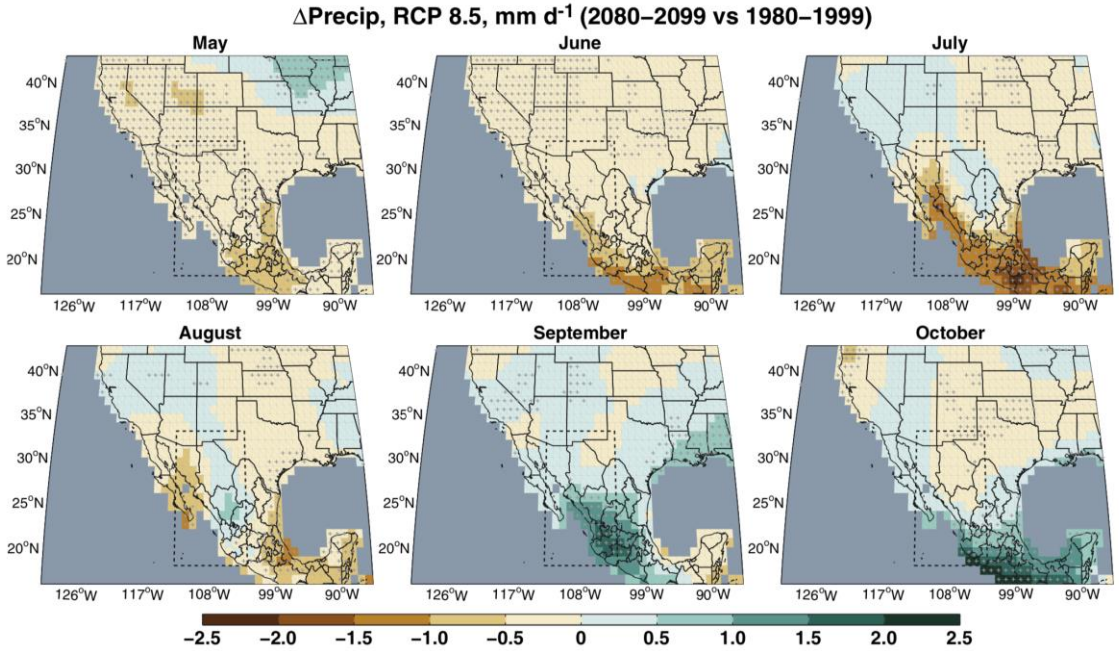

Figure 7. Multi-model mean precipitation differences (mm day^{-1}), calculated as mean precipitation for 2080-2099 (RCP 8.5 scenario) minus the mean precipitation for 1980-1999 (historical scenario) for the extended monsoon season (May-October). Core NAM region is outlined with the black dashed lines. Grey crosses indicate cells for which the sign of the change in at least 9 of the 11 models agrees with the sign of the change in the multi-model mean.

Cook and Seager (2013)

Global-scale analyses of the CMIP3 model projections for the twenty-first century indicate a strong, coherent decreased precipitation response over Central America and the Intra-America Seas region.

Fig. 9 Average summer (June–July–August) percent differences in precipitation, A1B (2061–2090)-20C (1961–1990). Positive (negative) values are in *green* (*brown*)

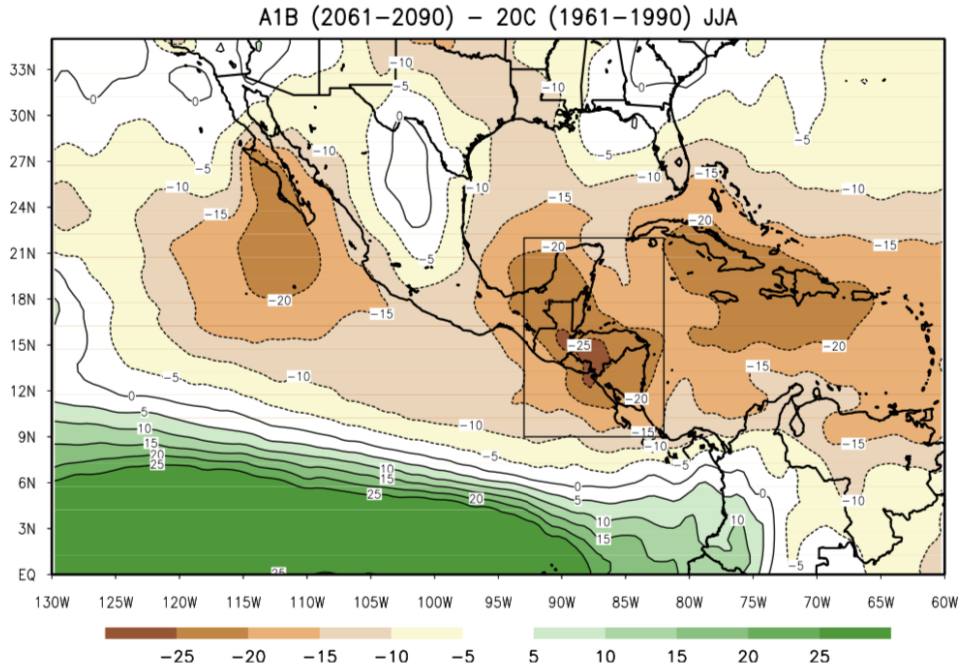

Fig. 10 Number of models with A1B-20C ensemble average precipitation differences greater than (less than) 0.1 (−0.1) mm day^{-1} in *green* (*brown*)

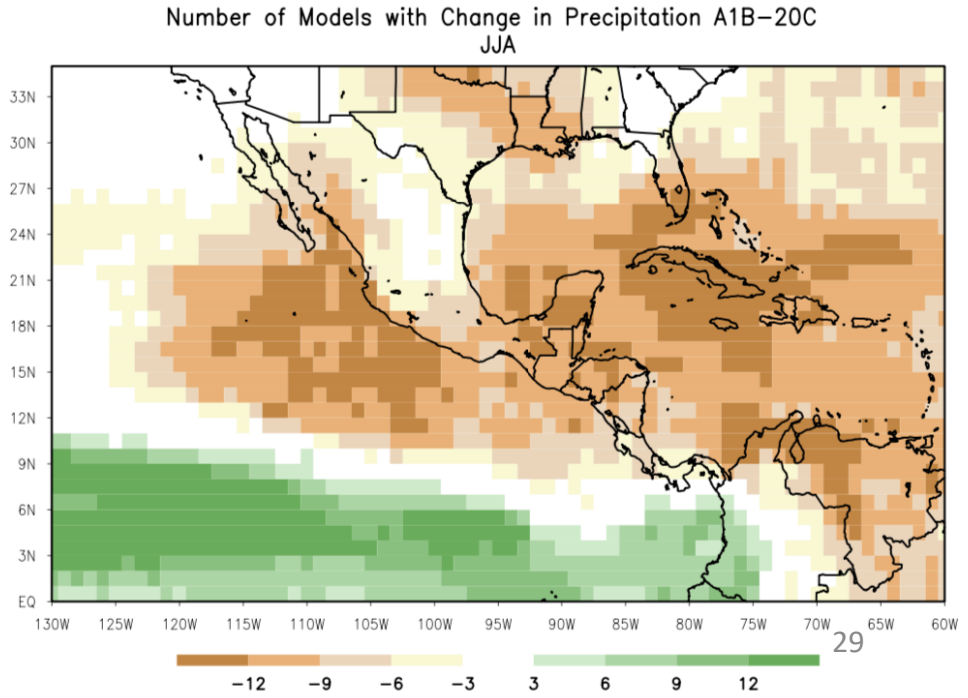

Rauscher et al. 2008

However, the monsoon response to GHG increases is sensitive to sea-surface temperature biases. When minimizing these biases, the model projects a robust reduction in monsoonal precipitation over the southwestern United States, contrasting with previous multi-model assessments.

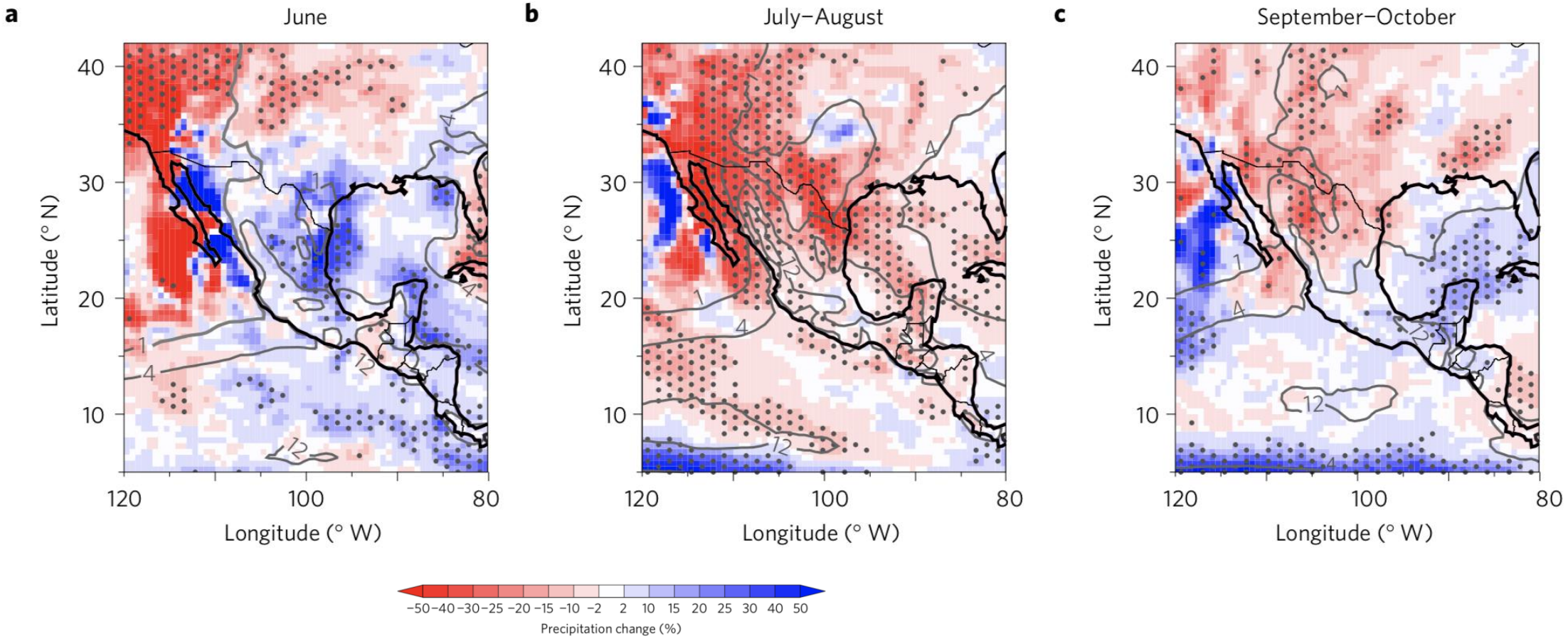

Figure 2 | Impact of increased CO_2 concentration and SST biases on the North American monsoon precipitation. a–c, Percentage precipitation change induced by CO_2 doubling in FLOR-FA simulations (%, colour shading; $2CO_2$_FLOR-FA minus CTRL_FLOR-FA) in June (**a**), July–August (**b**), and September–October (**c**). **d–f**, As in **a–c**, but for FLOR simulations ($2CO_2$_FLOR minus CTRL_FLOR). Grey contours denote climatological values of precipitation (mm d^{-1}) in the respective control runs. Stippling indicates regions where precipitation differences are statistically significant at the 5% level on the basis of a *t*-test.

Pascale et al. 2017

There are significant problems with GCM-based studies. In general, the Gulf of California is not adequately represented at coarser scales. There are also problems related to the convective parameterizations.

Both local and remote biases may lead to large uncertainties in the NAM projection under global warming.

GL	Seth et al. [129, 133]	GC, 1971–2100	Wet season delays; no precip. change
NAM	Cook and Seager [123]	GC, 1980–2100	Wet season delays; no precip. change
NAM	Torres-Alavez et al. [124]	GC, 1979–2099	Wet season delays; no precip. change
NAM	Maloney et al. [125]	GC, 1961–2099	Wet season delays; no precip. change
NAM	Pascale et al. [65]	GC, 1–200 CTL 301-500 2×CO_2	Sensitivity to SST biases and warming patterns; precip. reduction when SST biases removed
SW US	Pascale et al. [151]	GC, 1–200 CTL 301–500 2×CO_2	No change in the number of NAM surges; more extreme surge precip.; westward expansion of the NAM high
NAM	Bukovsky et al. [152]	RC, 1961–2069	Precip. reduction; increase in the heaviest precip. events
NAM	Meyer and Jin [64]	RC, 1979–2099	Sensitivity to SST biases and surface evaporation; precip. increase and earlier onset after removing SST biases
NAM,CA	Colorado-Ruiz et al. [126]	GC, 1979–2099	Intensification of midsummer drought
CA	Rauscher et al. [135]	GC, 1979–2099	Intensification of midsummer drought
CA	Fuentes-Franco et al. [136]	GC, 1979–2099	Intensification of midsummer drought
CONUS	Prein et al. [156]	RC, 2000–2013	Extreme precip. increasing with temp.

Pascale et al. 2019

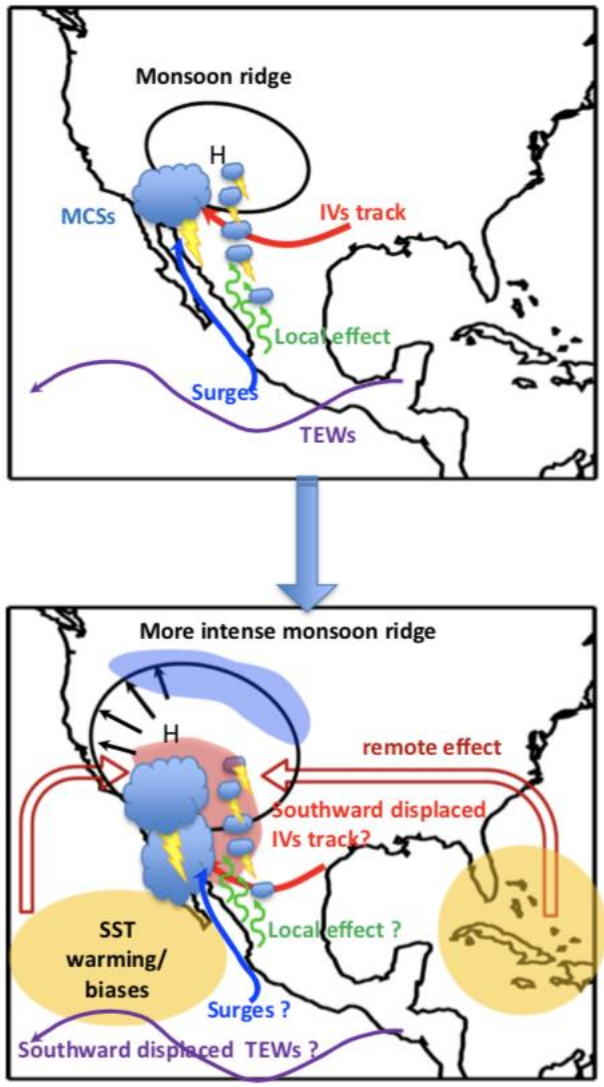

Changes in the NAM will depend on remote (e.g. warming of oceans) and local (land surface) processes.

For the NAM, some of the projected processes are the expansion and northwest- ward shift of the NAM ridge, the southward shift of the upper-level inverted troughs (IVs) track, and the strengthening of the remote stabilizing effect due to SST warming.

The thermodynamic atmospheric background is changing and becoming more favorable for extreme precipitation.

Pascale et al. 2019

Thus, there is an urgent need to address the systematic SST biases in GCMs, and enhance the realism of their land surface parameterizations.

What will large-scale shifts implicate for transient weather systems that are ultimately shaping the diurnal cycle of convection?

We need to reduce the uncertainty associated with the response to greenhouse warming of the MJO and ENSO to better define the future of the NAM at the seasonal and interannual timescales.

Pascale et al. 2019